Natural and artificial ageing in aluminium alloys – the role of excess vacancies

Zi Yang and John Banhart

Helmholtz-Centre Berlin for Materials and Energy, Hahn-Meitner-Platz 1, 14109 Berlin, Germany

Supplementary Material

S1. Parameters used for the simulations

The parameters related to solute diffusion used in the simulations are all taken from Mantina et al. [1]. They were calculated by first principles using the local density approximation to density functional theory, see Table. S1. The atomic jump frequencies w_k, $k = 0..4$, are calculated from Eq. (4) of Ref. [1] the correlation factor f_2 from Eqs. (2, 3) of Ref. [1] for a given temperature and atom species.

Table S1. Diffusion parameters as taken from Mantina et al. [1].

atom i	$\Delta H_{f,0} / \Delta S_{f,0}$	$\Delta H_{m,0}$	v_0^*	$\Delta H_{m,k}^i$ (k=1..4)	$v_k^{*,i}$ (k=1..4)	$\Delta H_b^i / \Delta S_b^i$
	(eV) / (k_B)	(eV)	(THz)	(eV)	(THz)	(eV) / (k_B)
Al	0.71 / 1.21	0.58	16.6			
Mg				0.68	21.8	−0.07 / −0.27
				0.42	18.6	
				0.50	13.3	
				0.57	17.1	
Si				0.52	10.9	0.11 / 0.44
				0.55	15.7	
				0.66	22.3	
				0.55	13.7	
used in Eqs.	(5,7): x_{v-eq} (6): $\widetilde{D}_{eq}$	(6): $\widetilde{D}_{eq}$		(3): w_2, f_2 (6): $\widetilde{D}_{eq}$	(3): w_2, f_2 (6): $\widetilde{D}_{eq}$	(8): $x_{v-eq,trp}^i$ (6): $\widetilde{D}_{eq}$

$\Delta H_{f,0}, \Delta S_{f,0}$:   free (index '0') vacancy **f**ormation enthalpy and entropy, $\Delta G_{f,0} = \Delta H_{f,0} - T \Delta S_{f,0}$

$\Delta H_{m,0}, (\Delta S_{m,0})$: free (index '0') vacancy **m**igration enthalpy*

$\Delta H_{m,k}^i (\Delta S_{m,k}^i)$: solute **m**igration enthalpy* of the 5 jumps and species i. k=2 is solute-vacancy exchange. k=0 represents vacancy migration in the free Al lattice, hence $\Delta H_{m,0}^i = \Delta H_{m,0}$ for all i.

$v_k^{*,i}$ effective frequency in transition state theory (TST) (v_0^*: fully in Al matrix)

$\Delta H_b^i, \Delta S_b^i$:   solute-vacancy **b**inding enthalpy and entropy, $\Delta G_b^i = \Delta H_b^i - T \Delta S_b^i$ for species i

* migration entropies also available from Ref. [2] but not used here to maintain consistency of data.

The average diffusion coefficient $\widetilde{D}_{eq}$ is calculated by:

$$\widetilde{D}_{eq} = a^2 \left(\left(1 - \sum_i c^i\right) f_0 \cdot v_0^* \cdot e^{-\frac{\Delta H_{m,0}}{kT}} + \sum_i c^i f_2^i \cdot v_2^{*,i} \cdot e^{-\frac{\Delta H_{m,2}^i}{kT}} e^{\frac{\Delta G_b^i}{kT}} \right) e^{-\frac{\Delta H_{f,0}}{kT}} e^{\frac{\Delta S_{f,0}}{T}}.$$

Vacancy trapping by clusters is guided by the following considerations:

- Vacancy-cluster interaction energy ΔH_b^{cl}: 0.2 eV at onset of ageing, 0.306 eV after short ageing (α=0.2), 0.581 eV after advanced ageing ($\alpha\sim$0.7) (energy values from Ref. [3], α values estimated),

- Cluster number density increases linearly from 0 to 6×10^{24} m^{-3} (i.e. site fraction c^{cl} from 0 to 10^{-4}) during ageing.

Hence the parametrisation: $\Delta H_b^{cl} = (0.2 + 0.53\ \alpha)$ [eV] and $c^{cl} = 10^{-4}\ \alpha$ is applied.

Table S2. Further parameters in calculations.

a	R	n_{jog}	n_d	n_p	f_0	T_{cs}	dT/dt
0.405 nm	25 µm	3.7×10^{19} m^{-3}	7.5×10^{11} m^{-2}	50	0.7815	200 °C	1000 Ks^{-1}

a:	lattice constant of aluminium
R:	grain radius (determined by light microscopy)
$n_{jog} = \frac{n_d}{n_p a}$:	jog density derived from dislocation density n_d and jog spacing n_p. This value is not very well known. $n_d = 10^{11}$ m^{-2} has been used in a previous calculations [4], $n_d = 3\times10^{11}$ m^{-2} by others including the current author's group [5, 6]. In Ref. [5] it was noted that such a value explained initial quenching from 540 °C well, but that subsequent operations at lower temperatures, e.g. at 180 °C, indicated a markedly higher value. Possibly, n_d changes during thermal processing. The value chosen here is deemed a compromise between various cases. The quantity n_p is also not known precisely. Values of 100 have been given based on theoretical considerations [7]. As n_p can be compensated by n_d without changing the relevant quantity n_{jog}, there is a lot of space for finding values.
f_0:	fcc correlation factor (=0.7815)
T_{cs}:	cluster start temperature. Determines that during initial quenching from the solutionising temperature, precipitation does not set in above T_{cs} in accordance with experimental findings in Ref. [8]. Variations of this value within the margin set by other sources (160 °C as calculated by Ref. [9], 175 °C and possibly higher for excess Mg [10]) have only a very small effect on results.
dT/dt:	average quenching rate from the solutionising temperature (540 °C) to 0 °C. The temperature course applied is a decaying exponential so that the cooling rate is initially higher.

S2. Equations of the trapping model

Temporary trapping of vacancies by solute atoms is an important ingredient of the model applied. We follow the formalism proposed by Lomer and extend the model by optional trapping by clusters (all of equal size).

Among N lattice sites we distinguish between sites where vacancies are adjacent ('trapped') to one of the solute atoms i, site fraction c^i, $z = 12$ neighbouring sites, or adjacent to one of the clusters containing N^{cl} atoms each and having site fractions c^{cl} and with z^{cl} neighbouring sites, or at the remaining matrix sites. The number of vacancies in equilibrium in each of the three cases is given by the vacancy formation free enthalpy $\Delta G_{f,0} = \Delta H_{f,0} - T\Delta S_{f,0}$, see Table S1:

$$N_{v-eq,mat} = N \exp\left(-\frac{\Delta G_{f,0}}{kT}\right)\left(1 - (z+1)\sum_i c^i - (z^{cl} + N^{cl})c^{cl}\right) \tag{S1}$$

$$N_{v-eq,trp}^i = N \exp\left(-\frac{\Delta G_{f,0}}{kT}\right) z c^i \exp\left(\frac{\Delta G_b^i}{kT}\right) \tag{S2}$$

$$N_{v-eq,trp}^{cl} = N \exp\left(-\frac{\Delta G_{f,0}}{kT}\right) z^{cl} c^{cl} \exp\left(\frac{\Delta H_b^{cl}}{kT}\right) \tag{S3}$$

The total number of vacancies anywhere is then the sum of the three:

$$N_{v-eq} = N_{v-eq,mat} + \sum_i N_{v-eq,trp}^i + N_{v-eq,trp}^{cl} = N \exp\left(-\frac{\Delta G_{f,0}}{kT}\right) \times$$

$$\underbrace{\left(1 - (z+1)\sum_i c^i - (z^{cl} + N^{cl})c^{cl}\right) + \sum_i z c^i \exp\left(\frac{\Delta G_b^i}{kT}\right) + z_{cl} c^{cl} \exp\left(\frac{\Delta H_b^{cl}}{kT}\right)}_{L} \tag{S4}$$

The term under the brace we call the 'Lomer factor', L

By dividing the numbers in Eqs. (S1, S2) by the number of matrix or trap sites we obtain the probability of a matrix or trap site of being occupied by a vacancy:

$$x_{v-eq,mat} = \frac{N_{v-eq,mat}}{N\left(1-(z+1)\sum_i c^i - (z^{cl}+N^{cl})c^{cl}\right)} = \exp\left(-\frac{\Delta G_{f,0}}{kT}\right) \tag{S5}$$

= *local* site fraction in matrix wrt. actual matrix lattice sites excluding lattice sites around solutes or clusters, and

$$x_{v-eq,trp}^i = \frac{N_{v-eq,trp}^i}{Nzc^i} = \exp\left(-\frac{\Delta G_{f,0} - \Delta G_b^i}{kT}\right) \tag{S6}$$

= *local* site fraction around solute of type i wrt. actual trap lattice sites. In analogy $x_{v-eq,trp}^{cl}$.

Hence:

$$x^i_{v-eq,trp} = x_{v-eq,mat} \exp\left(\frac{\Delta G^i_b}{kT}\right), \tag{S7}$$

By dividing the numbers in Eqs. (S1-S3) by the total lattice sites N, *average* site fractions are obtained, which receive the letter y:

$$y_{v-eq,mat} = \frac{N_{v-eq,mat}}{N} = \left(1 - (z+1)\sum_i c^i - (z^{cl} + N^{cl})c^{cl}\right) \underbrace{\exp\left(-\frac{\Delta G_{f,0}}{kT}\right)}_{x_{v-eq,mat}} \tag{S8}$$

$$y^i_{v-eq,trp} = \frac{N^i_{v-eq,trp}}{N} = zc^i \underbrace{\exp\left(-\frac{\Delta G_{f,0}}{kT}\right)\exp\left(\frac{\Delta G^i_b}{kT}\right)}_{x^i_{v-eq,trp}} \tag{S9}$$

$$y^{cl}_{v-eq,trp} = \frac{N^{cl}_{v-eq,trp}}{N} = z^{cl}c^{cl} \underbrace{\exp\left(-\frac{\Delta G_{f,0}}{kT}\right)\exp\left(\frac{\Delta H^{cl}_b}{kT}\right)}_{x^{cl}_{v-eq,trp}} \tag{S10}$$

And therefore

$$y_{v-eq} = \frac{N_{v-eq,mat} + \sum_i N^i_{v-eq,trp} + N^{cl}_{v-eq,trp}}{N} = \exp\left(-\frac{\Delta G_{f,0}}{kT}\right) \times L \tag{S11}$$

The total equilibrium vacancy site fraction in a defect-free lattice, $\exp\left(-\frac{\Delta G_{f,0}}{kT}\right)$, is therefore increased by the Lomer factor. Note that the y quantities do not have to be calculated in the simulation, thus they are not introduced in the main paper. They are shown here to present the conservation of total vacancies during vacancy trapping and repartitioning since only these quantities can be summed up in the style of Eq. (S11). For the total vacancy site fraction we have:

$$y_{v-eq} = x_{v-eq} \tag{S12}$$

By inserting Eq. (S9) into Eq. (S11) we obtain the inverse Lomer equation Eq. (8) in the main paper used for determining $x^i_{v-eq,trp}$ to be used in the precipitation equation (3). It is not restricted to equilibrium, which is why we drop the index 'eq':

$$x^i_{v,trp} = \frac{\exp\left(\frac{\Delta G^i_b}{kT}\right)}{L} x_v \tag{S13}$$

The calculations in Secs. 4.2. and 4.3 are carried out without cluster trapping, i.e. all terms indexed with "cl" in above equations are neglected. In Eq. (S1) we tacitly assume that the decreasing number of solute atoms and the associated trapping is implicitly compensated by increasing cluster trapping.

In Sec. 4.4 we include cluster trapping explicitly. The four cluster-related quantities z^{cl}, N^{cl}, c^{cl} and ΔH_b^{cl} are treated in reasonable approximations:

- $z^{cl} = z = 12$, i.e. the cluster is treated as a point like defect
- $(z^{cl} + N^{cl})c^{cl}$ in Eq. (S1) is neglected because $c^{cl} \ll c^i$
- c^{cl} and ΔH_b^{cl} are assumed to increase continuously with the progress of clustering based on reported cluster number densities/site fractions and vacancy-cluster binding energies, see main paper and Sec. S1 above.

In order to avoid double counting of trapping sites, we replace all terms c^i in above equations by $c^i(1 - \alpha^i)$. Thus, as cluster trapping increases, solute trapping decreases, both linearly with progressing clustering.

Francis and Curtin have derived equations for the trapping of vacancies by a single solute type with the objective of engineering the vacancy site fraction [11]. Their results are based on more general and exact thermodynamic considerations than those by Lomer but contain Lomer's equations as a limiting case. Their Eqs. (5a, 5b) describe the concentration of vacancies not associated to a solute and those in the vicinity of solute atoms at thermal equilibrium and correspond to above Eqs. (S8, S9), respectively. This can be seen by considering only single vacancies, hence $\eta = z + 1 = 13$ in their equations. Next, their definition of the solute-vacancy binding energy differs from ours by the sign. Replacing the absolute energy of solute-vacancy complexes in their Eqs. by the binding energy we obtain

'concentration of vacancies in the matrix': $\qquad c_V = y_{v-eq,mat}$

'concentration of solute/vacancy complexes': $\qquad c_i = \dfrac{y_{v-eq,trp}^i}{1 + \dfrac{y_{v-eq,trp}^i}{c^i}} \approx y_{v-eq,trp}^i \qquad (S14)$

Where only on the l.h.s of these equations the notation of Ref. [11] is used. In the denominator of the latter equation $\frac{y_{v-eq,trp}^i}{c^i} = z\, x_{v-eq,trp}^i$ using Eq. (S8, S9). $x_{v-eq,trp}^i$ never exceeds 4×10^{-4} as shown in Fig. 4a and hence the denominator is very close to 1.

S3. The pre-factor p_{att}

Eq. (2) contains a dimensionless pre-factor p_{att} that we have assumed to be constant throughout the calculations. Its value has been fixed to **8×10^{-6}** since at this value the ageing curves are divided into an excess and equilibrium part in roughly the same proportions as observed experimentally.

For example, the height of the clustering peak in the DSC curves in Fig. 6a is about 1/3 of that of the high-temperature peak and in Fig. 4d, approximately the same ratio is observed between first and second reaction (horizontal line) in accordance with the experiments. p_{att} describes how likely it is that a diffusing solute atom reaches a target and forms a complex with it, after which the vacancy detaches again and is available for further diffusion.

Clearly, the site fraction of the target objects is part of p_{att}. For solute atoms, it ranges around $c = 5 \times 10^{-3}$ for the alloy considered here. As solutes are replaced by clusters it might drop as clustering proceeds but we keep to the initial value. Therefore, the pre-factor used splits up into $p_{att} = 5 \times 10^{-3} \times 0.0016 = 8 \times 10^{-6}$. The remaining unexplained factor 0.0016 contains the attachment probability and possibly other factors.

The attachment of solutes to other solutes is a complicated process governed by a range of interaction energies. A recent first-principle calculation of these energies between 2 atoms (Mg,Si) and one vacancy specifies 7 configurations and next neighbour and second next neighbour values that range from 0.01 to 0.14 eV [12]. The actual attachment might go through various steps, possibly also involving interaction energies between more distant objects that can be repulsive in some cases [13]. The attachment probability would then depend on a combination of such energies and be temperature dependent. We currently have no formalism to calculate such a scenario, but the average value of 0.0016 for the remaining factor does not seem unlikely. Our choice of p_{att}, although adjusted to experiments, is compatible with some qualitative assumptions of cluster formation.

S4. Maximum precipitation caused by excess vacancies

We now calculate the maximum precipitated fraction caused by excess vacancies as a function of ageing temperature. For simplicity, only one solute type and no vacancy trapping by clusters is considered in the calculation. The objective is to support interpretation of the numerical results in Fig. 4d by identifying elementary quantities that lead to the behaviour observed there.

First, the total increase of α can be written as

$$\alpha = \alpha_{ex} + \alpha_{eq}, \tag{S15}$$

where subscripts 'ex' and 'eq' represent the fractions caused by excess vacancies and equilibrium vacancies, respectively. Similarly, at any moment the local vacancy site fraction at a site around solutes can be considered a sum of equilibrium and excess vacancy site fractions:

$$x_{v,trp} = x_{v-ex,trp} + x_{v-eq,trp}, \tag{S16}$$

where $x_{v-eq,trp}$ is calculated using Eq. (S7). Combining Eqs. (S7, S15, S16) and Eqs. (3, 7) of the main paper, we obtain

$$\frac{d\alpha_{ex}}{dt} = A \cdot (1 - \alpha) \cdot f_2 \cdot v_2^* \cdot e^{-\frac{\Delta H_{m,2}}{kT}} \cdot e^{\frac{\Delta G_b}{kT}} \cdot \left(x_{v,mat} - x_{v-eq,mat}\right). \tag{S17}$$

Next, we calculate $x_{v,mat}$ from the kinetic Eq. (6) of the main paper. Note that $x_{v-eq} = L \cdot x_{v-eq,mat}$ in Eq. (6), where L is the 'Lomer factor' based on vacancy trapping by solutes.

Integrating Eq. (6) for x_v for isothermal ageing at temperature T, and applying $x_{v,mat} = \frac{x_v}{L}$, we obtain

$$x_{v,mat} = x_{v-eq,mat} \cdot \left(\frac{x_{v,0}}{L \cdot x_{v-eq,mat}}\right)^{e^{-\left(\frac{15}{R^2} + 2\pi a n_{jog}\right)\frac{\tilde{D}_{eq}}{f_0 \cdot L \cdot x_{v-eq,mat}} t}} \tag{S18}$$

where $x_{v,0}$ is the initial total vacancy fraction before ageing, which is lower than the equilibrium fraction at 540 °C as some vacancies are lost during quenching. As $t \to \infty$, $x_{v,mat} \to x_{v-eq,mat}$.

Now, we combine Eqs. (S17, S18) to integrate α_{ex}. Since the initial site fraction is several orders of magnitude higher than the equilibrium fraction, $\alpha_{eq} \ll \alpha_{ex}$ is valid till $x_{v,mat}$ is very low, after which the increase in α_{ex} can also be neglected. Therefore we apply an approximation $\alpha \cong \alpha_{ex}$ in Eq. (S17) for the calculation of α_{ex}. Thus, we obtain

$$\alpha_{ex} = 1 - e^{\left[-A \cdot f_2 \cdot v_2^* \cdot e^{-\frac{\Delta H_{m,2}}{kT}} \cdot e^{\frac{\Delta G_b}{kT}} \cdot \int_0^\infty (x_{v,mat} - x_{v-eq,mat}) dt\right]}$$

$$= 1 - e^{\left[-\frac{A f_0 x_{v,0}}{\left(\frac{15}{R^2} + 2\pi a n_{jog}\right)a^2} \cdot \frac{D_2}{\tilde{D}_{eq}} \cdot L \cdot x_{v-eq,mat} \cdot \left\{Ei\left[\ln\left(\frac{x_{v,0}}{L \cdot x_{v-eq,mat}}\right)\right] - \gamma - \ln\left[\ln\left(\frac{x_{v,0}}{L \cdot x_{v-eq,mat}}\right)\right]\right\}\right]}, \tag{S19a}$$

where Ei is the exponential integral function and γ is the Euler-Mascheroni constant, and where

$$D_2(T) = a^2 \cdot f_2 \cdot v_2^* \cdot e^{-\frac{\Delta H_{m,2}}{kT}} \cdot e^{\frac{\Delta G_b}{kT}} \cdot x_{v-eq,mat}.$$

Eq. (S19a) can be condensed to

$$\alpha_{ex}(T) = 1 - e^{\left[-B \cdot \frac{D_2(T)}{\tilde{D}_{eq}(T)} \zeta(T)\right]} \tag{S19b}$$

by defining $B = \frac{A f_0 x_{v,0}}{\left(\frac{15}{R^2} + 2\pi a n_{jog}\right)a^2}$,

and $\zeta(T) = L \cdot x_{v-eq,mat} \cdot \left\{Ei\left[\ln\left(\frac{x_{v,0}}{L \cdot x_{v-eq,mat}}\right)\right] - \gamma - \ln\left[\ln\left(\frac{x_{v,0}}{L \cdot x_{v-eq,mat}}\right)\right]\right\}$.

These quantities are given in Fig. 8a of the main paper. The temperature dependence of Eq. (S19b) = Eq. (9) of the main paper determines the broken line in Fig. 4b and reflects the hardening anomaly.

S5. Additional graphs that help to understand details of calculation

In the following, we show some aspects of the simulations not mentioned in the main paper.
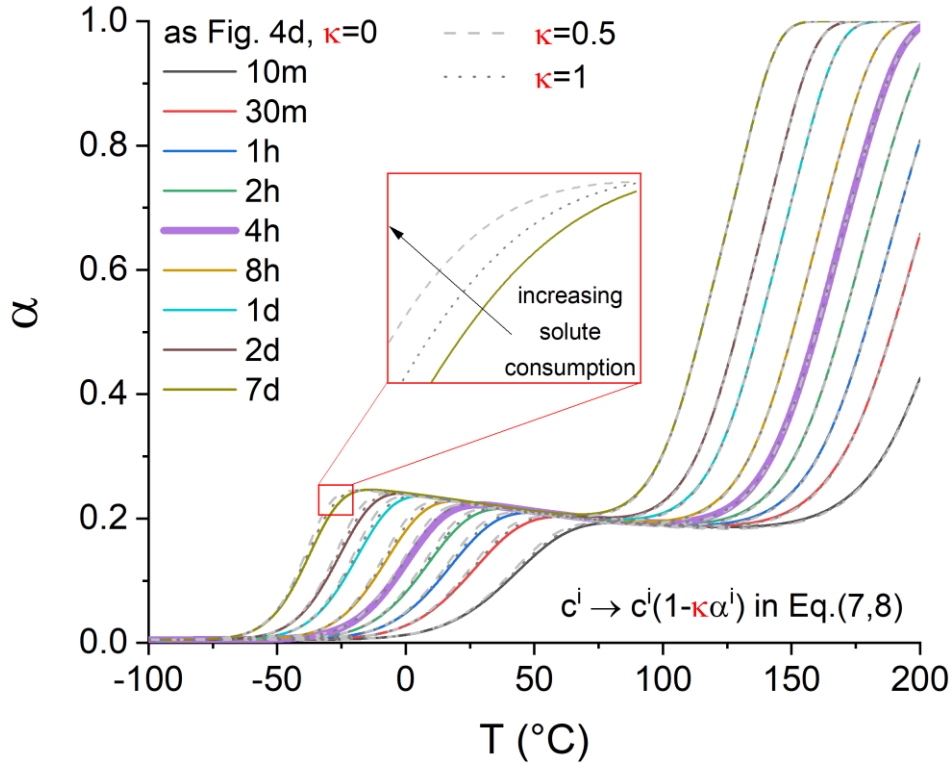

Fig. S1. Data presented in Fig. 4d and data calculated in addition with a correction for solute consumption due to clustering in Eq. (7, 8) using the ansatz $c^i = c^i_{\text{initial}}(1 - \kappa^i \alpha^i)$, where κ is the fraction of solute atoms that after final ageing has been transferred into clusters and precipitates. Atom probe experiments suggest κ^i values between 0.15 and 0.25 for NA and short AA [14-16], but as very small clusters might not be detected as such κ^i could be higher. However, the calculation suggests that application of a correction does hardly influence the results. We therefore assume $c^i = c^i_{\text{initial}}$ in all the calculations to avoid introduction of additional parameters.
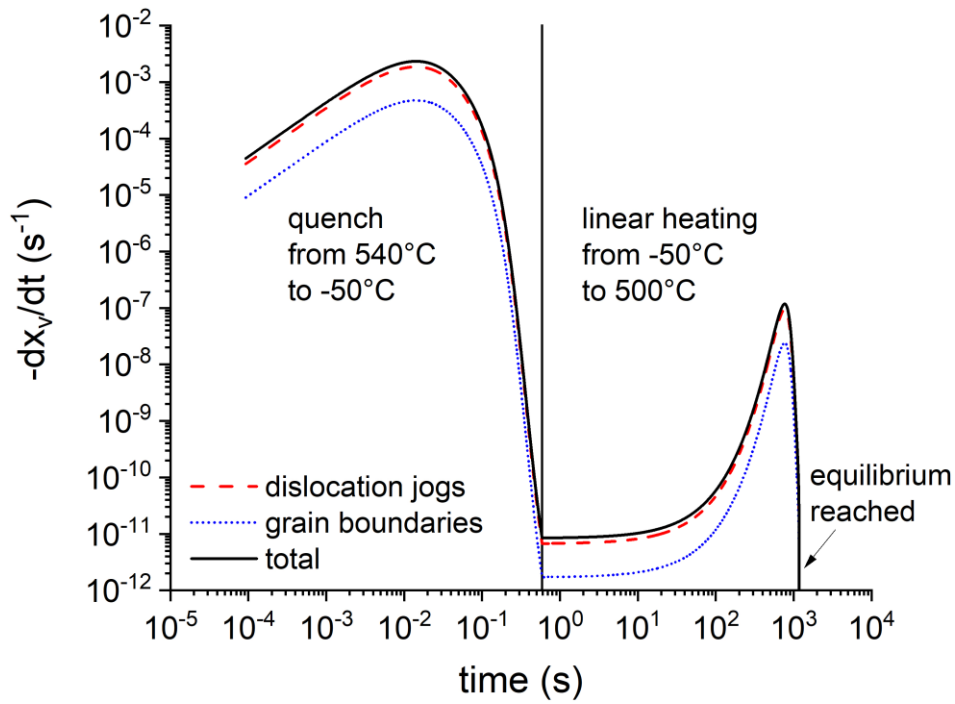
Fig. S2. Derivatives of x_v in the vacancy annihilation model during quenching and subsequent linear heating. 'dislocation jogs' and 'grain boundaries' refer to the two contributions in Eq. (6) of the main paper that remain at a constant fraction during ageing, the first being about 6 times higher. In the pure ternary alloys with their mm-sized grains as compared to the more fine grained alloy 6014 (50 μm grain diameter) in Figure 3 of the main paper, the vacancy annihilation rate would therefore be marginally smaller, provided that the density of dislocation jogs was the same.
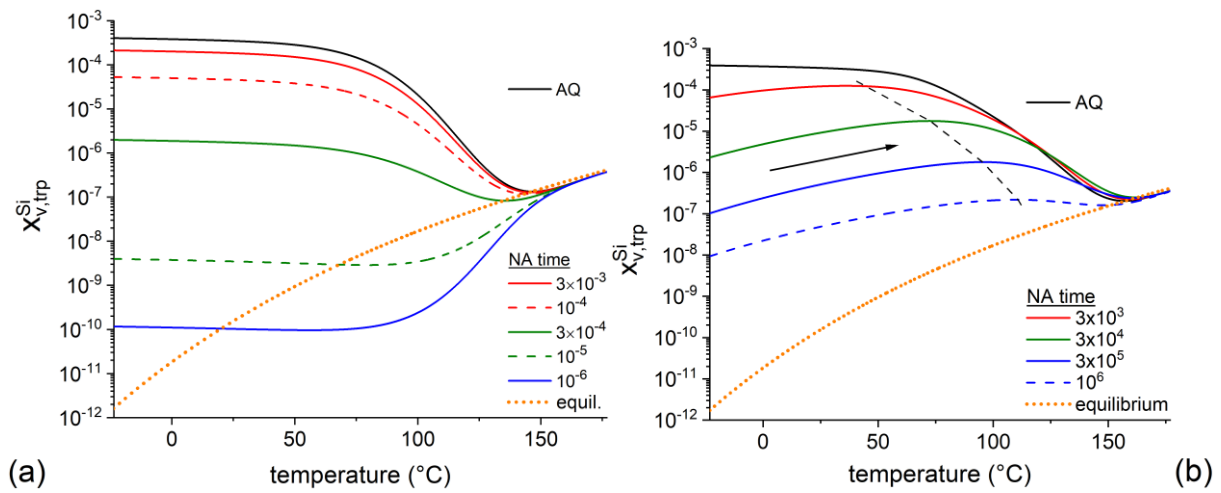
Fig. S3. Calculated vacancy site fraction at Si sites during constant heating at 10 K·min^{-1}. (a) After NA at 20°C for various times without vacancy trapping by clusters, (b) same with trapping by clusters included, see Sec. 4.4. Without trapping by clusters in a), the vacancy site fraction is reduced to 10^{-10} after 10^6 s during NA, whereas in the presence of trapping by clusters this reduction is less pronounced (b). Moreover, in a), during subsequent linear heating the vacancy site fraction decreases towards the equilibrium value (orange line) at the respective temperature, whereas in b) the vacancy site fraction increases for a limited period delimited by the broken line. The reason is that after long NA (e.g. 3×10^5 s), 99.5% of all he vacancies are trapped by clusters and only 0.5% are at Si sites (2×10^{-4} are free), hence the slow diffusion. Linear heating releases vacancies from clusters and brings them into solution (6%) or into vacancy-Si complexes (9%).
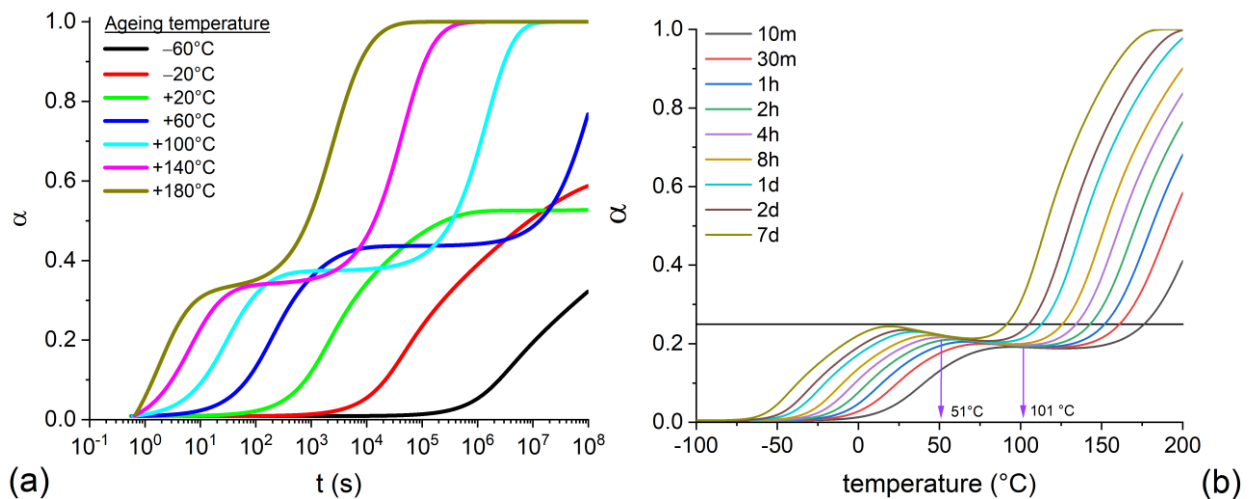

Fig. S4. Analogous to Figs. 4c,d, but with vacancy-cluster interactions enabled as described in Sec. 4.4. The main effect is to make the curves appear flatter.
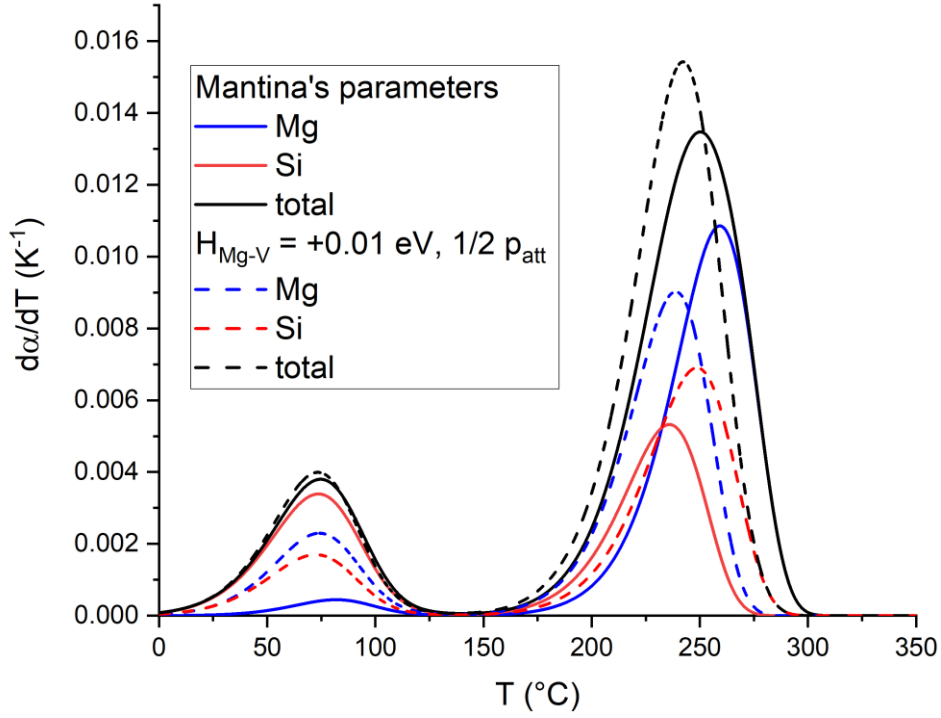
Fig. S5. Effect of a change of binding energy between Mg and vacancies ΔH_b^{Mg} from -0.07 eV (Mantina's value used in this paper) to 0.01 eV (value suggested by Ref. [12]). Other parameters are still the ones given by Mantina, see Table S1. Therefore, the modified parameter set is not entirely consistent any more. The pre-factor p_{att} has been reduced to ½ of the original value thus ensuing that the clustering peak still has roughly the same height. The total precipitation course during linear heating (black lines) differs mainly in the high-temperature region. However, we see a shift of clustering activity from Si to Mg caused by the stronger trapping of vacancies by Mg atoms and the correspondingly enhanced Mg diffusion and precipitation. Most importantly, the dual structure of an excess-vacancy related low-temperature peak and a well separated high-temperature peak is not affected. Therefore, even if the binding energies are allowed to vary the conclusions of this paper remain valid.
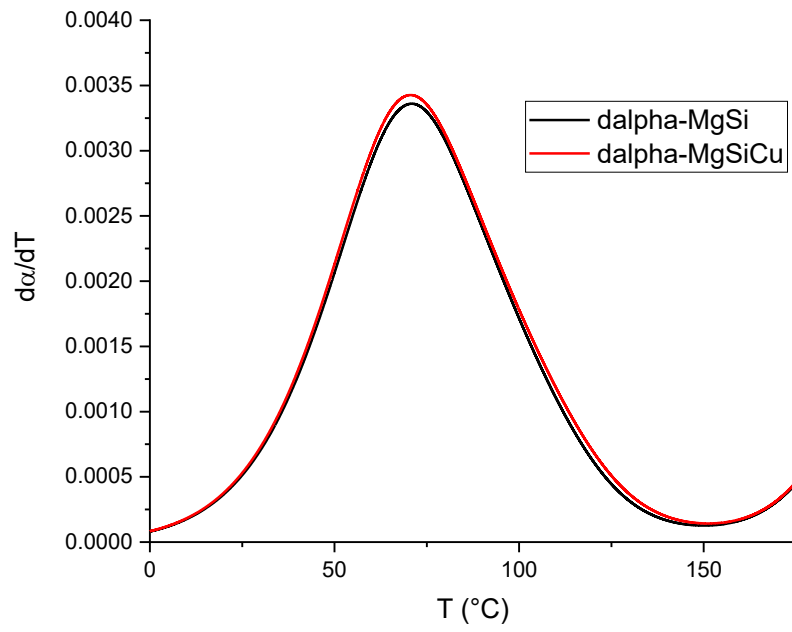
Fig. S6. Fig. 7c of the main paper recalculated with the addition of 0.12 wt.% Cu using the diffusion data given by Ref. [1] as for Mg and Si. The influence of Cu diffusion is very small.

References

[1]   M. Mantina, Y. Wang, L.Q. Chen, Z.K. Liu, C. Wolverton, First principles impurity diffusion coefficients, Acta Materialia 57 (2009) 4102-4108.

[2]   M. Mantina, Y. Wang, R. Arroyave, S.L. Shang, L.Q. Chen, Z.K. Liu, A first-principles approach to transition states of diffusion, Journal of Physics-Condensed Matter 24 (2012) 305402.

[3]   A. Jain, A. Glensk, D. Marchant, M. Ceriotti, W.A. Curtin, Vacancy prisons and solute clustering in aluminium alloys, International Conference on Aluminium Alloys ICAA, Oral presentation, 2020.

[4]   P. Dumitraschkewitz, P.J. Uggowitzer, S.S.A. Gerstl, J.F. Löffler, S. Pogatscher, Size-dependent diffusion controls natural aging in aluminium alloys, Nature Communications 10 (2019) 4746.

[5]   M. Madanat, M. Liu, X.-P. Zhang, Q.-N. Guo, J. Cizek, J. Banhart, Co-evolution of vacancies and solute clusters during artificial ageing of Al-Mg-Si alloys, Physical Review Materials 4 (2020) 063608.

[6]   A. Falahati, P. Lang, E. Kozeschnik, Precipitation in Al-alloy 6016 - the role of excess vacancies, Materials Science Forum 706-709 (2012) 317-322.

[7]   A.J. Ardell, H. Reiss, W.D. Nix, Statistics of jogs on dislocations at equilibrium, Journal of Applied Physics 36 (1965) 1727-1732.

[8]   Z. Yang, X.H. Jiang, X.-P. Zhang, M. Liu, Z.Q. Liang, D. Leyvraz, J. Banhart, Natural ageing clustering under different quenching conditions in an Al-Mg-Si alloy, Scripta Materialia 190 (2021) 179–182.

[9]   M.J. Starink, L.F. Cao, P.A. Rometsch, A model for the thermodynamics of and strengthening due to co-clusters in Al-Mg-Si-based alloys, Acta Materialia 60 (2012) 4194-4207.

[10]   A. Poznak, R.K.W. Marceau, P.G. Sanders, Composition dependent thermal stability and evolution of solute clusters in Al-Mg-Si analyzed using atom probe tomography, Materials Science and Engineering A 721 (2018) 47-60.

[11]   M.F. Francis, W.A. Curtin, Microalloying for the controllable delay of precipitate formation in metal alloys., Acta Materialia 106 (2016) 117-128.

[12]   J. Peng, S. Bahl, A. Shyam, J.A. Haynes, D.W. Shin, Solute-vacancy clustering in aluminum, Acta Materialia 196 (2020) 747–758.

[13]   T. Saito, E.A. Mortsell, S. Wenner, C.D. Marioara, S.J. Andersen, J. Friis, K. Matsuda, R. Holmestad, Atomic Structures of Precipitates in Al-Mg-Si Alloys with Small Additions of Other Elements, Advanced Engineering Materials 20 (2018).

[14]   J. Buha, R.N. Lumley, A.G. Crosky, K. Hono, Secondary precipitation in an Al-Mg-Si-Cu alloy, Acta Materialia 55 (2007) 3015-3024.

[15]   L.F. Cao, P.A. Rometsch, M.J. Couper, Effect of pre-ageing and natural ageing on the paint bake response of alloy AA6181A, Materials Science and Engineering A 571 (2013) 77-82.

[16]   M.W. Zandbergen, Q. Xu, A. Cerezo, G.D.W. Smith, Study of precipitation in Al-Mg-Si alloys by atom probe tomography I. Microstructural changes as a function of ageing temperature, Acta Materialia 101 (2015) 136-148.